

A. PETRARU^{1,✉}
V. NAGARAJAN²
H. KOHLSTEDT^{1,3}
R. RAMESH³
D.G. SCHLOM⁴
R. WASER¹

Simultaneous measurement of the piezoelectric and dielectric response of nanoscale ferroelectric capacitors by an atomic force microscopy based approach

¹ Institut für Festkörperforschung and CNI, Forschungszentrum Jülich GmbH, Jülich, Germany
² School of Materials Science and Engineering, University of New South Wales, Sydney, NSW 2052, Australia
³ Department of Materials Science and Engineering and Department of Physics, University of California, Berkeley, CA 94720 USA
⁴ Department of Materials Science and Engineering Pennsylvania State University, University Park, PA 16802 USA

Received: 18 August 2005 / Accepted: 14 March 2006
Published online: 8 April 2006 • © Springer-Verlag 2006

ABSTRACT We present a sensitive method to simultaneously acquire the $C(V)$ characteristics and piezoresponse of sub-micron size ferroelectric capacitors using an Atomic Force Microscope (AFM). Model Pt/(La_{0.5},Sr_{0.5})CoO₃/PbZr_{0.4}Ti_{0.6}O₃/(La_{0.5},Sr_{0.5})CoO₃/La:SrTiO₃/Si nanocapacitors were fabricated by focused ion beam milling from 100 μm² down to 0.04 μm². With this AFM based capacitance measurement technique we show clear “double-humped” $C(V)$ for all sizes with no significant change in the peak value of the ϵ_r down to capacitors with the smallest area of 0.04 μm². The smallest capacitance measured is only of the order a few femtofarads, demonstrating the high sensitivity of the technique. Simultaneously, the piezoelectric response is recorded for each measurement, thus the technique facilitates simultaneous piezoresponse and dielectric characterization of ferroelectric memory devices.

PACS 77.55.+f; 77.90.+k; 85.50.-n; 77.84.-s

1 Introduction

Recently ferroelectric thin films have been investigated in detail for use in sensing and nonvolatile memory applications [1]. Nonvolatile ferroelectric random access memories (NVRAMs) have many attractive properties such as low power consumption, long endurance and fast access times, which make them ideal for high density memory applications. However to make NVRAMs superior to current non-volatile memory candidates such as Flash, it is critical to scale the size of the ferroelectric cell down to nanoscale dimensions. Thus, the ability to successfully characterize ferroelectric properties of the small area capacitors, in the range of tens to hundreds of nanometers is of paramount importance. It is not surprising therefore, that in the past few years, there has been tremendous progress in the use of atomic force microscopy (AFM) based techniques to investigate ferroelectric behavior. This includes direct hysteresis loop measurements [2, 3], polarization switching experiments [4, 5] and piezoresponse domain

imaging studies [6–9]. Other methods based on the Sawyer–Tower circuit have also been proposed [10] to measure micron sized capacitors. Further, two current mode methods, constant current (CC) and triangular current (TC) based on charging of the ferroelectric capacitor were reported [11, 12] for measuring micron size ferroelectric capacitors.

Concurrent current detection in picoampere and lower levels has made tremendous progress. The use of lock-in based current detection technique has been presented by Oh et al. [13] Impedance detection methods have also been investigated. Shao et al [14] and later on O’Hayre et al. [15] have reported an advanced impedance based AFM technique to detect small amounts of currents. It is believed that the use of impedance based techniques removes the phase error inherent to lock-in based techniques and hence improves accuracy. However Lee et al. have shown a lock-in based very sensitive local capacitance technique [16] where capacitance values as low as attofarads could be detected. This method uses a bridge circuit and contains a bucking circuit to cancel the stray capacitive current. Very few of the above have been applied to the dielectric measurements of nanoscale ferroelectric/dielectric capacitors. Measurements of the dielectric response of the nanoscale ferroelectric capacitors are important because they can give us immense information such as scaling of the coercive voltage (generally the peaks of the “double-humped” curve), tunability of the ferroelectric layer, presence of passive layers etc. Although well established scanning probe techniques such as scanning capacitance microscopy [17], have been used to investigate the dielectric response of ferroelectrics at the nanoscale [18], extracting accurate quantitative information on the capacitance is still a challenge. In addition, often the parasitic capacitance is several hundred times larger than the device capacitance, thereby impeding the measurement of the true capacitance of the device. At the same time it is often desirable to measure more than one functional property. It has been hypothesized that understanding the dielectric response of nanoscale capacitors can give many hints on the scaling of other ferroelectric properties. In ferroelectrics particularly, it is known that the piezoelectric constants are strongly linked to the dielectric and the polarization behavior. For example, the tunability of the dielectric coefficient

✉ Fax: +49-2461-612550, E-mail: a.petraru@fz-juelich.de

is strongly dependent on the shape of the polarization curve. Similarly, often a high dielectric coefficient is also a signature of high piezoelectric coefficients. Thus an approach that could measure both the piezoelectric and dielectric behavior simultaneously would be of immense potential. In this paper, we demonstrate an approach that allows the simultaneous quantitative measurement of the $C(V)$ curve (capacitance versus voltage) and piezoresponse hysteresis loops for sub-micron sized ferroelectric capacitors. Our setup is shown to work very well for capacitors with an area down to $0.04 \mu\text{m}^2$ and capacitances down to a few femtofarads (10^{-15} F) after parasitic subtraction.

2 Experimental

Figure 1a shows a sketch of the system. The measurement setup consists of an atomic force microscope (AFM), a waveform generator (Agilent Technologies) and two lock-in amplifiers (Stanford Research Systems). The AFM used in this experiment was a Veeco Multimode equipped with a conductive Pt-Ir coated cantilever. The AFM tip and the base electrode are connected to the measurement setup via short wires to avoid increasing the parasitic capacitance and to minimize noise. The instrument is operated in contact mode, thus there is a firm contact between the conductive tip and the top electrode. The current to voltage convertor built into the lock-in amplifier may induce a change in the phase of the signal which is more pronounced at high frequencies. Therefore, a phase adjustment is required for each frequency prior to the measurement. Thus, in open circuit conditions (tip lifted), the phase is adjusted until the resistive part of the current becomes zero. One other approach for phase adjustment is to use an etalon resistor of for example, $50 \text{ M}\Omega$. The waveform generator is used to supply a sinusoidal signal with a variable DC offset. The two lock-in amplifiers and the waveform generator are controlled by a computer. The equivalent circuit is depicted in Fig. 1b. The parasitic capacitance of the setup C_{para} arising from cantilever-sample capacitance and wiring, is in parallel with the ferroelectric capacitor. The small signal current

measured by the first lock-in amplifier is given by:

$$i = i_R + j(i_{\text{para}} + i_{\text{fe}}), \quad (1)$$

where i_R is the resistive part, i_{para} is from the parasitic capacitance, i_{fe} is from ferroelectric capacitance and j denotes $\sqrt{-1}$. This current has an in-phase component i_R and an out-of-phase component $(i_{\text{para}} + i_{\text{fe}})$, which is 90° shifted with respect with the excitation signal.

The small signal capacitance is given by

$$C = \frac{\langle i_{\text{para}} \rangle_{\text{rms}} + \langle i_{\text{fe}} \rangle_{\text{rms}}}{2\pi\nu \langle u \rangle_{\text{rms}}} \quad (2)$$

where ν is the small signal frequency; the rms values of i , u are taken. In order to find the ferroelectric capacitance, the parasitic capacitance has to be subtracted from the total capacitance. More details on how the parasitic capacitance is computed is given later on.

The dynamic resistance

$$R(U) = \left. \frac{\Delta u}{\Delta i} \right|_{U=\text{const.}} = \frac{\langle u \rangle_{\text{rms}}}{\langle i_R \rangle_{\text{rms}}} \quad (3)$$

is also acquired and it gives information about the leakage current of the ferroelectric capacitors. For piezoresponse measurements, a second lock-in amplifier receives the signal from the optical detector of the AFM. Thus, the out-of-plane deflection of the laser beam modulated by the excitation signal via the converse piezoelectric effect is recorded, and it is proportional to the corresponding piezoelectric coefficient (d_{33} in the case of c -axis oriented $\text{Pb}(\text{Zr},\text{Ti})\text{O}_3$ epitaxial films). A quartz plate can be used as a calibration sample for converting the signal from the optical detector of the AFM to a displacement. The piezoelectric response and the electrical measurements are performed simultaneously. In this letter we focus on the absolute measurements of the dielectric response of the nanocapacitors as the scaling of the piezoresponse has been reported in detail elsewhere by several other reports.

Details on the ferroelectric test structures chosen for this experiment are given elsewhere [19]. In short, epitaxial $\text{PbZr}_{0.4}\text{Ti}_{0.6}\text{O}_3$ films were prepared by sol-gel deposition with top and bottom sputtered $(\text{La}_{0.5},\text{Sr}_{0.5})\text{CoO}_3$ oxide electrodes on La-doped SrTiO_3 (epitaxial conductive template layer) buffered Si substrate. The nominal thickness of the ferroelectric layer was 120 nm. Capacitors with varying sizes from $100 \mu\text{m}^2$ to $0.04 \mu\text{m}^2$ were fabricated via focused Ga ion beam milling (FIB) followed by annealing in an oxygen furnace at 500°C to eliminate ion beam damage.

In Fig. 2 we plot the raw capacitance data obtained for the smallest capacitor (from now on referred to as a nanocapacitor). The area of the nanocapacitor is $0.04 \mu\text{m}^2$, measured via AFM topography scans and reconfirmed by SEM images. A SEM picture of a capacitor of this size is shown in Fig. 4c. The loop (line) clearly shows a double-humped curve, thus indicating the ferroelectric nature of the nanoisland. We note that the capacitance value, as measured, is of the order of hundreds of femtofarads. A simple back-calculation of the dielectric constant using the above capacitance value leads to an unusually large dielectric constant in the range 10^5 – 10^6 . The main source of this error in the $C(V)$ measurements of

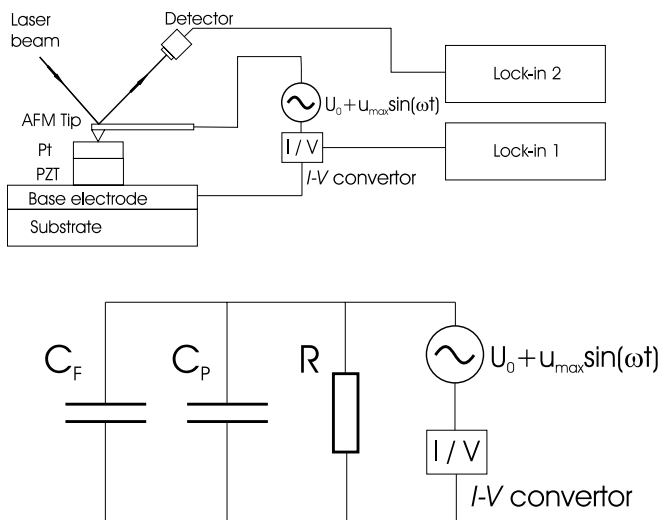


FIGURE 1 (a) Experimental arrangement for simultaneously measuring $C(V)$ and piezoresponse of the ferroelectric capacitors. (b) Equivalent circuit

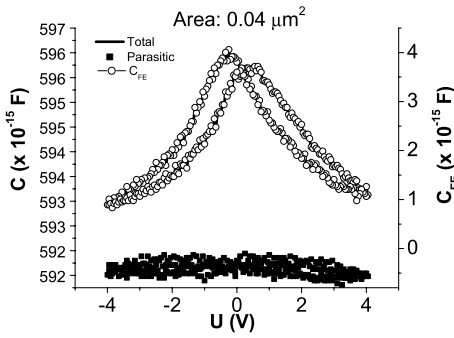


FIGURE 2 $C(V)$ for a capacitor with an area of $0.04 \mu\text{m}^2$: total capacitance, parasitic capacitance and ferroelectric capacitance

the nanocapacitors comes from the presence of high parasitic capacitance (compared to the capacitance of interest). While the parasitic capacitance is negligible in comparison with that of the ferroelectric capacitors for areas higher than $25 \mu\text{m}^2$, it becomes significant in the case of sub- μm size devices. In order to determine the actual value of dielectric constant of the nanocapacitors it is therefore important to determine very accurately the parasitic capacitance in order to subtract it from the total capacitance. The traditional method to do this is to lift the tip such that the circuit is open, and conduct the measurement again. However recent simulations [3] show that this technique is not very accurate, and the measured parasitic is strongly dependent on the height to which the tip is lifted. Therefore this method does not lead to an unambiguous measurement of the parasitic capacitance. Ideally the most true measurement of the parasitic capacitance is to use the same tip after it has lost the conductive coating from the very top and perform the measurement again. In this case the ferroelectric capacitor is disconnected from the circuit and precise parasitic capacitance is determined. Since this is not a practical solution (but good for checking

the setup), our approach was to move the tip laterally, outside the milled electrode area (since the surrounding area is insulating) and then to measure the parasitic capacitance. Another approach is to adjust the set-point for the AFM feedback loop until the electrical contact between the tip and the capacitor is lost, but the cantilever is still in the proximity of the sample surface. This measurement of the parasitic capacitance is shown with dots in Fig. 2. For the experimental set-up discussed in this paper, the value of the parasitic is in the range of 592 fF. We find that it is strongly linear, and deducting this from our raw data yields the true capacitance of the device. This is shown as the dotted points in Fig. 2. The total capacitance is plotted with a continuous line. The shape of the true $C(V)$ loop (open circles) is the same, however it's magnitude has now dropped to only a few femtofarads after parasitic subtraction. It is also interesting to point out that in our $C(V)$ measurements the magnitude of the coercive voltage (obtained from the position of the peaks in the double humped curve) does not change after parasitic subtraction. This is in strong contrast to polarization hysteresis measurements where the coercive voltages before and after the parasitic subtractions can vary significantly [2]. The major limiting factor of this technique is the parasitic capacitance. Since the parasitic capacitance mostly consists of the cantilever-sample capacitance, small size cantilevers are therefore recommended for nanocapacitors measurements.

Figure 3 shows the $C(V)$ together with the piezoresponse hysteresis loop for several device areas: $100 \mu\text{m}^2$, $25 \mu\text{m}^2$, $9 \mu\text{m}^2$ and $0.09 \mu\text{m}^2$. The small signal frequency for these measurements was 10 KHz and the small signal amplitude was $0.7 V_{pp}$. For all the measurements presented here, the sweeping of the DC offset starts from zero volt, then goes to $+V_{max}$, $-V_{max}$ and ends at zero, thus closing the loop. This is illustrated in Fig. 3a with arrows along the d_{33} hysteresis loop.

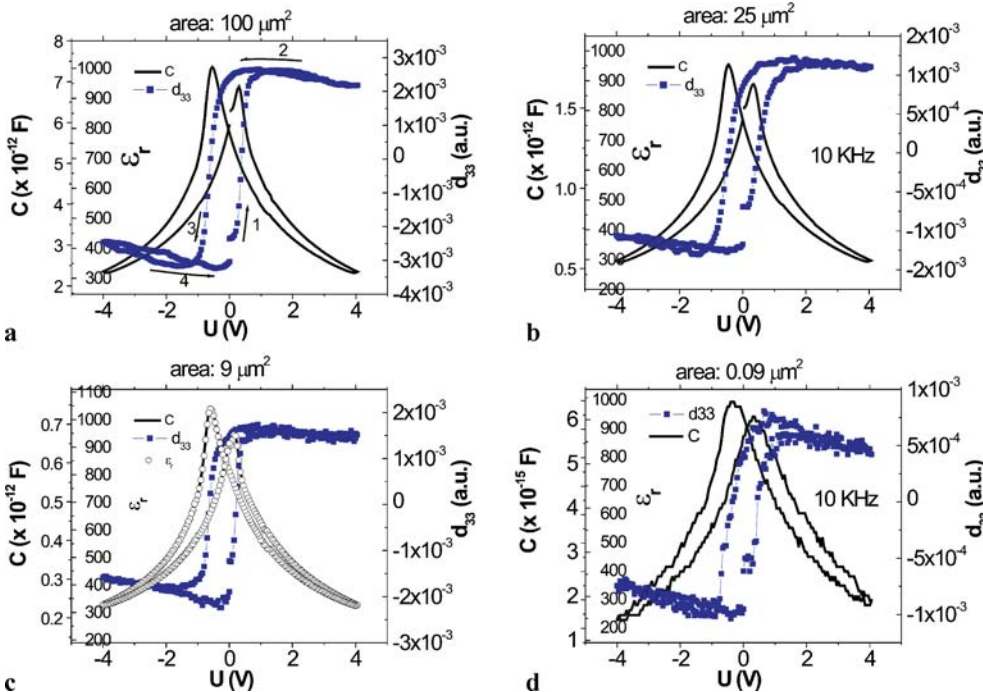


FIGURE 3 Simultaneous measurements of the capacitance and piezoresponse of FIB PZT thin film capacitors having different areas

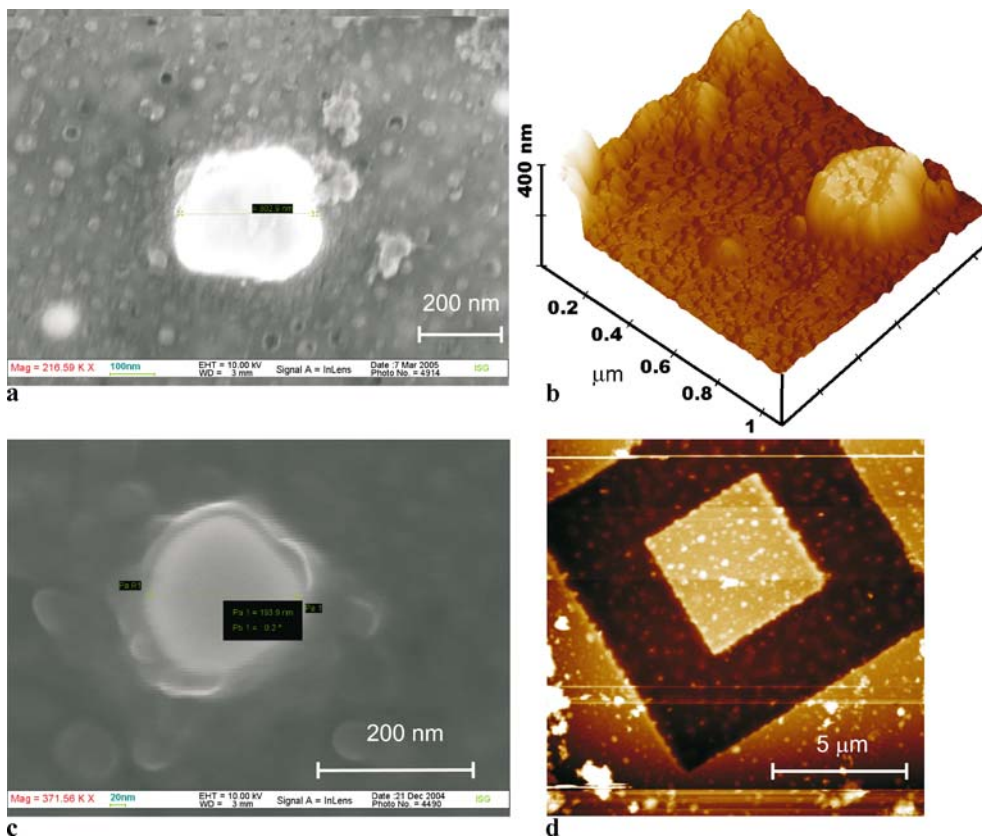


FIGURE 4 (a, b) AFM and SEM images of a ferroelectric capacitor with an area of $0.09 \mu\text{m}^2$; (c) SEM image of a $0.04 \mu\text{m}^2$ ferroelectric capacitor – the smallest area in this study; (d) AFM picture of a $25 \mu\text{m}^2$ area capacitor

The total time for acquiring a complete loop was 53 s. The value of the ϵ_r was derived assuming parallel-plate capacitors. The area of the capacitors was measured using AFM topography scans and SEM images. Some of these pictures are shown in Fig. 4. Our measured peak values of the relative permittivity ϵ_r are comparable with those reported in [11] for PZT films with a slightly different composition ($\text{PbZr}_{0.3}\text{Ti}_{0.7}\text{O}_3$), measured with the constant current method. We find that the coercive voltages measured from the d_{33} loops are the same as that obtained from the $C(V)$ curves (within error). Moreover the peak positions do not change with device size, suggesting an absence of scaling of the coercive voltage (and hence coercive field) with lateral dimensions, in contrast to the strong scaling shown by the coercive voltage when the thickness of the ferroelectric is varied. We do not find a significant variation in the tunability of the dielectric constant but we observe a broadening of the peak of the dielectric constant with decreasing size.

In Fig. 5 we plot the peak dielectric constant as a function of the capacitor area. The error bars represent a combination of the errors in the measurement of the area and statistical variation in the data. Within these error bars we find no significant variation of the dielectric constant. The peak value is approximately 1000, in agreement with previous reports for the same kind of ferroelectric material. Normally smaller pads show an increase in their piezoelectric constant compared to larger clamped capacitors. Based on these results the dielectric constant was expected to also increase, therefore we find the above trend surprising. More detailed investigations into the dielectric behavior of the ferroelectric layer as a function of size are therefore necessary.

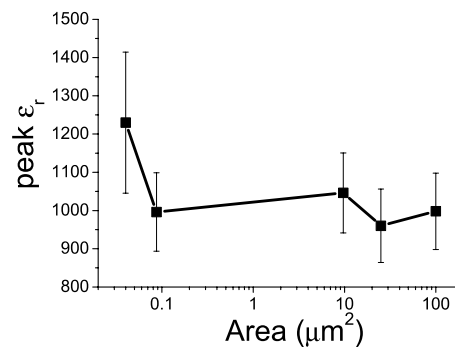


FIGURE 5 Peak dielectric constant as a function of the capacitor area

ACKNOWLEDGEMENTS We wish to thank Dr. A. Stanishevsky for the fabrication of the nanocapacitors and Mr. S. Kronholz for the SEM images. This work was supported by Volkswagen-Stiftung (www.volkswagenstiftung.de) within the program “Complex Materials: Co-operative Projects of the Natural, Engineering, and Biosciences” under the title: “Nano-sized ferroelectric Hybrids” under project number I/77 737. V. N thanks the Humboldt Stiftung for his stay in Germany. We also thank the NSF-DFG joint program for financial support.

REFERENCES

- O. Auciello, J.F. Scott, R. Ramesh, Phys. Today **51**, 22 (1998)
- S. Tiedke, T. Schmitz, K. Prume, A. Roelofs, T. Schneller, U. Kall, R. Waser, C.S. Ganpule, V. Nagarajan, A. Stanishevsky, R. Ramesh, Appl. Phys. Lett. **79**, 3678 (2001)
- T. Schmitz, K. Prume, B. Reichenberg, A. Roelofs, R. Waser, S. Tiedke, J. Eur. Ceram. Soc. **24**, 1145 (2004)
- S. Prasertchoung, V. Nagarajan, Z. Ma, R. Ramesh, J. S. Cross, M. Tsukada, Appl. Phys. Lett. **84**, 3678 (2004)
- C. Dehoff, B.J. Rodriguez, A.I. Kingon, R.J. Nemanich, A. Gruverman, J.S. Cross, Rev. Sci. Instrum. **76**, 023 708 (2005)

- 6 A. Gruverman, O. Auciello, H. Tokumoto, *Ann. Rev. Mater. Sci.* **28**, 101 (1998)
- 7 C.S. Ganpule, A.L. Roytburd, V. Nagarajan, B.K. Hill, S.B. Ogale, E.D. Williams, R. Ramesh, J.F. Scott, *Phys. Rev. B* **65**, 014101 (2001)
- 8 I. Stolichnov, A. Tagantsev, N. Setter, J.S. Cross, M. Tsukada, *Appl. Phys. Lett.* **86**, 3362 (2003)
- 9 T. Tybell, P. Paruch, T. Giamarchi, J.-M. Triscone, *Phys. Rev. Lett.* **89**, 97601 (2002)
- 10 R. Bouregba, B. Vilquin, G. Le Rhun, G. Poullain, B. Domenges, *Rev. Sci. Instrum.* **74**, 4429 (2003)
- 11 D.-Y. Wang, C.-Y. Chang, *Jpn. J. Appl. Phys.* **43**, 4263 (2004)
- 12 D.-Y. Wang, C.-Y. Chang, *Jpn. J. Appl. Phys.* **43**, 6225 (2004)
- 13 J. Oh, R.J. Nemanicha, *J. Appl. Phys.* **92**, 3326 (2002)
- 14 R. Shao, S.V. Kalinin, D.A. Bonnell, *Appl. Phys. Lett.* **82**, 1869 (2003)
- 15 R. OHayre, M. Lee, F.B. Prinz, *J. Appl. Phys.* **95**, 8382 (2004)
- 16 D.T. Lee, J.P. Pelz, B. Bhushan, *Rev. Sci. Instrum.* **73**, 3525 (2002)
- 17 C.C. Williams, W.P. Hough, S.A. Rishton, *Appl. Phys. Lett.* **55**, 203 (1989)
- 18 C.C. Leu, C.Y. Chen, C.H. Chien, M.N. Chang, F.Y. Hsu, C.T. Hu, *Appl. Phys. Lett.* **82**, 3493 (2003)
- 19 B.T. Liu, K. Maki, Y. So, V. Nagarajan, R. Ramesh, J. Lettieri, J.H. Haeni, D.G. Schlom, W. Tian, X.Q. Pan, F.J. Walker, R.A. McKee, *Appl. Phys. Lett.* **80**, 4801 (2002)